MIT Libraries | DSpace@MIT

MIT Open Access Articles

Microfluidic rheometry

The MIT Faculty has made this article openly available. ***Please share*** how this access benefits you. Your story matters.

Citation: Pipe, Christopher J., and Gareth H. McKinley. "Microfluidic Rheometry." Mechanics Research Communications 36, no. 1 (January 2009): 110–120.

As Published: http://dx.doi.org/10.1016/j.mechrescom.2008.08.009

Publisher: Elsevier

Persistent URL: http://hdl.handle.net/1721.1/99349

Version: Author's final manuscript: final author's manuscript post peer review, without publisher's formatting or copy editing

Terms of use: Creative Commons Attribution-Noncommercial-NoDerivatives

Massachusetts Institute of Technology

Microfluidic rheometry

Christopher J. Pipe [a,*], Gareth H. McKinley [b,*]

[a] *State Key Laboratory of Nonlinear Mechanics, Institute of Mechanics, Chinese Academy of Sciences, Beijing 100190, P.R. China*

[b] *Hatsopoulos Microfluids Laboratory, Department of Mechanical Engineering, Massachusetts Institute of Technology, Cambridge, MA 02139, USA*

Abstract

The development and growth of microfluidics has stimulated interest in the behaviour of complex liquids in microscale geometries and provided a rich platform for rheometric investigations of non-Newtonian phenomena at small scales. Microfluidic techniques present the rheologist with new opportunities for material property measurement and this review discusses the use of microfluidic devices to measure bulk rheology in both shear and extensional flows. Capillary, stagnation and contraction flows are presented in this context and developments, limitations and future perspectives are examined.

Key words: Microfluidics, Rheology, Rheometry, Shear viscosity, Extensional viscosity, Capillary flow, Stagnation point flow, Contraction flow

* Corresponding author.
Email addresses: `chris@lnm.imech.ac.cn` (Christopher J. Pipe), `gareth@mit.edu` (Gareth H. McKinley).

Preprint

1 Introduction

Over the past decade the study of flows in geometries with characteristic length-scales of less than 100 μm has flourished (Stone et al., 2004; Whitesides, 2006). Developments in techniques for investigating and manipulating such flow configurations have been driven by recent advances in micro-fabrication techniques allowing the cheap and reliable manufacture of geometries with micron-scale feature resolution (Quake and Scherer, 2000; Ng et al., 2002; Marrian and Tennant, 2003) combined with the trend of miniaturization in the biotechnology, manufacturing and chemical processing industries. Common microfluidic device applications include coating flows, formation of suspensions, emulsions and foams, heat transfer and flows in lab-on-a-chip devices (Obot, 2002; Hansen and Quake, 2003; Stone et al., 2004; Squires and Quake, 2005). Many of these ultimate applications involve handling fluids that have a complex microstructure and the flow of these materials may give rise to non-Newtonian phenomena (Bird et al., 1987; Larson, 1999). In order to optimize the design and implementation of microfluidic systems, a detailed understanding of the bulk flow of complex liquids on small scales is clearly desirable.

Classical macroscopic rheometry techniques for measuring fluid properties in shear and elongation typically involve characteristic length-scales $O(1\,\mathrm{mm})$, require sample volumes $O(1\,\mathrm{ml})$ and probe deformation rates of perhaps up to $O(100-1000\,\mathrm{s}^{-1})$ (Macosko, 1994; Petrie, 2006). While these methods are satisfactory for understanding the behaviour of many fluids in a wide variety of flows, there are circumstances when using devices with smaller length-scales to investigate rheological response may be advantageous. These include exploring sensitivity to interfacial conditions, probing large deformation rates

Preprint

in the absence of inertia or viscous heating, measuring flow phenomena when device length-scales approach those of the underlying material microstructure and the possibility of studying sample volumes on the order of nanolitres. Straightforward adaptations of classical macro-scale devices to incorporate micrometric length-scales has been shown to be effective for measuring shear properties under certain conditions; however, it becomes necessary to incorporate large correction factors to compensate for flow non-idealities (Connelly and Greener, 1985; Duda et al., 1988; Pipe et al., 2008) or to develop advanced opto-mechanical sub-systems to ensure precise alignment (Dhinojwala and Granick, 1997; Clasen and McKinley, 2004). Moving down to molecularly thin films of complex liquids, atomic force microscopy (MacKintosh and Schmidt, 1999) and surface force apparatus instruments (Mukhopadhyay and Granick, 2001) have been used to study nano-scale rheology (Meyer et al., 1998); however, once again severe instrument artifacts can overwhelm the observations (McKenna, 2006). Despite the strong impetus driving the miniatuarization of rheometric instrumentation, the ability of macro-scale systems to probe the bulk rheology of a fluid at the micro-scale has remained limited, largely because shrinking down some mechanical subsystems such as torsional motors and torque transducers is impractical. The arrival of microfluidic technology, however, has opened significant new possibilities for exploring the behaviour of complex liquids in micron sized geometries: not only does it allow the precise, rapid and cheap development of small scale devices but it also provides the ability to integrate rheological devices with other microfluidic components for lab-on-a-chip devices, opening new lines of application.

We review some of these recent developments in the present article: among a range of techniques situated at the junction of microfluidics and rheology we

focus on the use of microfluidic devices to measure bulk rheological properties in shear and extensional flow. A very brief summary of other key approaches is given below and the reader is directed to the references provided for further information regarding these methods:

- ⋆ Particle-based methods can be used to estimate the local rheological response due to the motions of nanoscale particles (Waigh, 2005; Larson, 2007). Systems can be 'passively driven' where the motions of particles due to thermal fluctuations are analyzed (Weitz and Pine, 1992; Starrs and Bartlett, 2003) or 'actively driven' where forces exerted on beads are measured using optical traps (Meiners and Quake, 2000; Brau et al., 2007) or magnetic tweezers (Bausch et al., 1998).
- ⋆ The dynamics of single polymers, especially fluorescently-labeled DNA, freely undergoing shear or extensional flow can be directly observed under certain conditions (Perkins et al., 1997; Smith et al., 1999; Hur et al., 2001) and related to the macroscopic rheological response measured in conventional rheometers. The use of DNA solutions as a model polymer system for probing the dynamics of flexible chains in different flow types is reviewed comprehensively by Shaqfeh (Shaqfeh, 2005).
- ⋆ Microfluidic devices can also be used to control the creation of droplets in a repeatable manner (Thorsen et al., 2001; Anna et al., 2003; Link et al., 2004), allowing the dynamics of single or groups of droplets to be explored, an important step in understanding the rheology of multiphase liquids.
- ⋆ Microfluidic studies of ordered complex fluids, such as liquid crystals, can be used to impose well-defined structural and orientational boundary conditions on length-scales comparable to the dimensions of the observed order (Choi et al., 2004; Shojaei-Zadeh and Anna, 2006).

Preprint

This review is arranged in the following order: section 2 discusses microfluidic capillary techniques for measuring the steady shear viscosity; in section 3 we discuss microfluidic stagnation point flows; and in section 4 we examine microfluidic contraction flows for measuring extensional properties. Finally we examine perspectives for future work on microfluidic devices for investigating the rheology of complex liquids.

1.1 Device and fluid length-scales

We take the working definition for a microfluidic system as a device with at least one characteristic length-scale d in the range $1 \leq d \leq 100\,\mu$m. For complex liquids the continuum hypothesis is still considered to be valid at such length-scales, but this may not be the case for flows of gases when the ratio of the mean free path l_{f} to the smallest characteristic dimension is of order $l_{\mathrm{f}}/d \sim 0.001$ and compressibility becomes important (Colin, 2005). The microstructural length-scales of complex liquids, such as the radius of gyration of a polymer chain or a characteristic radius of a suspended particle, typically vary from 1 nm to 10 μm, and as such the working fluid may not be well approximated as microstructurally homogeneous. Additionally, as the characteristic length-scale of the flow geometry approaches that of the fluid microstructure, physical confinement can alter the dynamical evolution of the microstructure (Chen et al., 2004; Stein et al., 2006) and must be taken into account when considering the bulk response.

Preprint

1.2 Surface effects

The ratio of surface area S to volume V for a fluid element is proportional to $S/V \sim d^{-1}$ and therefore moving towards smaller characteristic length-scales increases the relative importance of surface interactions compared to the behaviour of the bulk. While the classical 'no-slip' hypothesis at a smooth solid-fluid interface is generally regarded valid down to length-scales 10 nm (Lauga et al., 2007), interactions at surfaces may lead to substantial apparent slip. Thus depletion layers are a potential source of non-homogeneity in the sample being investigated (Barnes, 1995; Granick et al., 2003) and may affect the measured rheological response. Apparent slip can be caused by surface roughness, the confining effect of the walls causing solute-poor regions near the wall, hydrophilic/hydrophobic interactions at interfaces and the influence of electrical properties in ionic liquids or liquids containing charged particles (Lauga et al., 2007; Voronov et al., 2008).

1.3 Relevant dimensionless groups

The small length-scales characteristic of microfluidic devices generally result in flows of liquids in which viscous stresses dominate inertia with typical Reynolds numbers $\mathrm{Re} = \rho U d/\eta < 1$, where η is the dynamic viscosity, ρ is the fluid density and U is a characteristic velocity of the flow which is controlled by the volumetric flow rate $U \sim Q/d^2$. While low Reynolds number flows present challenges that limit efficient mixing in microfluidic systems (Stroock et al., 2002), they are advantageous when seeking to impose laminar viscometric flows with controlled kinematics and, for Newtonian fluids at

Preprint

least, it is possible to accurately compute steady two-dimensional and three-dimensional flows (Oliveira et al., 2008). Microfluidic devices manufactured using conventional lithographic techniques are usually planar and for steady shearing flow in devices where the ratio of width w to depth d (see figure 1(a)) $w/d \gg 1$; classical lubrication approximations (Batchelor, 1967) can also be used to model many aspects of the flow field, except in regions where the geometry changes rapidly in the streamwise direction.

In microfluidic flows of complex liquids the Bond number $\mathrm{Bo} = \rho d^2 g/\sigma \ll 1$, where σ is the interfacial tension and g is the acceleration due to gravity, and capillary forces dominate body forces in the formation of fluid interfaces. Capillary forces are also usually large compared to viscous forces leading to capillary numbers $\mathrm{Ca} = \eta U/\sigma \ll 1$. Because capillary forces are so large in microfluidic devices dislodging air bubbles can be extremely problematic, and because the capillary length $l_{\mathrm{cap}} = (\sigma/\rho g)^{1/2}$ is an order of magnitude greater than device length-scales, residual air bubbles can substantially distort local flow profiles.

Many complex liquids used in microfluidic applications (for example solutions containing proteins, DNA or other biopolymers) exhibit viscoelastic relaxation times $\lambda \sim 10^{-3}$ s or smaller and therefore do not show extravagant viscoelastic phenomena in laminar macro-scale flows. It is thus difficult to measure the material functions that characterize the fluid rheology in a conventional rheometer. However, at the high deformation rates $\dot{\gamma} \sim U/d \sim Q/d^3$ which can be achieved in the absence of inertia using microfabricated geometries, large Deborah numbers $\mathrm{De} = \dot{\gamma}\,\lambda > 1$ become accessible and viscoelastic stresses may be significant.

Preprint

The increasing importance of understanding viscoelastic fluid effects as flow geometries are miniaturized is highlighted by the elasticity number $\mathrm{El} = \mathrm{De}/\mathrm{Re} = \lambda\eta/(\rho d^2)$; because both De and Re increase linearly with Q, the ratio is independent of flow rate and controlled by material properties and geometry. For a given viscoelastic liquid, increasing elastic effects are realized at smaller length-scales. This is especially noteworthy for low viscosity polymer solutions, for which the elasticity number may be $\mathrm{El} \ll 1$ in macroscopic flows, whereas in microscale geometries, flows with $\mathrm{El} \gg 1$ are possible (Rodd et al., 2005).

2 Microfluidic capillary devices

Capillary viscometry using macro-scale devices can be an extremely reliable and accurate technique for measuring shear viscosities (Macosko, 1994). The shear viscosity η is calculated as a function of the flow rate Q and pressure drop ΔP through a straight capillary of known dimensions (White, 1991), with axisymmetric or planar slit geometries commonly used. One seeks to measure a very low value of wall shear stress τ at a given shear rate $\dot{\gamma} \sim Q/(wd^2)$, where for a rectilinear channel w is the channel width, d is the channel depth and typically the aspect ratio $w/d \gg 1$. For steady fully-developed flow in a rectilinear channel the pressure drop is given by the force balance $wd\Delta P = 2L(w+d)\tau$, where L is the channel length. Hence the measured pressure drop $\Delta P = 2\tau L(w+d)/(wd) \sim 2\tau L/d$ which can be very large when $L/d \gg 1$ and $w/d \gg 1$. We note that this is in direct contrast to rotational-based rheometric systems where the measured torque $\mathcal{T} \sim 2\eta\pi R^2 L$ (with R the radius of the measuring fixture), can become very small when the device length-scales R and

L are reduced. Consequently microfluidic rheometry is naturally predisposed to exploiting the well-developed principles of capillary viscometry due to the inherent simplicity of the design combined with the ease of microfabricating straight planar channels with small depths compared to the channel length.

2.1 Principles of operation

A sketch of a prototypical planar microfluidic capillary viscometer is shown in figure 1(a). The fundamental principle employed by microfluidic capillary viscometers is identical to their macroscale counterparts and the shear viscosity is found from the pressure drop ΔP and flow rate Q for a capillary of length L. A key difference between conventional and microfluidic capillary viscometers, however, is that the former are often gravity-driven resulting in measurements of the kinematic shear viscosity $\nu = \eta/\rho$ while the latter give the dynamic shear viscosity η directly. For laminar Newtonian flow in a capillary the viscosity is given by $\eta = wd^3\Delta P/[2LkQ(1 + d/w)]$, where k is a numerical factor depending on the channel geometry; $k = 6$ for a slit channel ($w/d \gg 1$) and $k = 14.3$ for a square channel ($w/d = 1$). For fluids with a shear-rate dependent viscosity the Weissenberg–Rabinowitsch–Mooney equation for rectilinear channels is used to calculate the viscosity and in this case a factor of $[2 + \mathrm{d}(\ln Q)/\mathrm{d}(\ln \Delta P)]/3$ must be included (Macosko, 1994).

Two main approaches to microfluidic capillary viscometry can be identified: (a) imposing a pressure drop and measuring the flow rate (Srivastava et al., 2005; Lee and Tripathi, 2005; Degré et al., 2006; Guillot et al., 2006; Lin et al., 2007; Han et al., 2007; Masselon et al., 2008), and (b) imposing the flow rate and measuring the resulting pressure drop (Kang et al., 2005; Pipe et al., 2008).

Preprint

For pressure driven flows, a variety of methods have been exploited including capillary pressure (Srivastava et al., 2005), electrowetting (Lin et al., 2007), controlling upstream hydrostatic pressure (Degré et al., 2006; Guillot et al., 2006; Masselon et al., 2008) and decreased downstream pressure in a controlled volume of air as the gas is slowly absorbed into a porous PDMS elastomer (Han et al., 2007). Techniques for measuring the flow rate include micro particle image velocimetry (μPIV) (Degré et al., 2006; Guillot et al., 2006; Masselon et al., 2008) and the observation of the fluid free surface by video microscopy (Srivastava et al., 2005; Guillot et al., 2006; Lin et al., 2007; Han et al., 2007). The controlled-pressure microfluidic device of Lee and Tripathi (2005) enables direct measurement of the intrinsic viscosity of biopolymer solutions and the flow rate is evaluated by fluorescence intensity of the bulk flow.

In both of the controlled flow rate studies published to date the volumetric flow rate was imposed using a syringe pump and the pressure drop was monitored using either traditional pressure sensors (Kang et al., 2005) or microfabricated pressure sensors (Pipe et al., 2008). The potential issue of 'hole pressure corrections' (i.e. additional extra viscoelastic stresses arising from streamline curvature near the channel boundary (Higashitani and Pritchard, 1972)) can be circumvented either by using flush-mounted transducers or by directly measuring a differential pressure drop. In this latter case, the sensing elements are located at two geometrically identical wall locations; the extra viscoelastic stresses are then of identical magnitude at both locations and cancel each other out in the differential measurement (Rodd et al., 2005). The theoretical paper of Zimmerman et al. (2006) proposes a wholly different approach whereby the pressure opposite the entrance to a T-junction is measured and the shear viscosity for shear-thinning fluids can thus be calculated.

Preprint

The current capabilities of both imposed rate and imposed pressure techniques are illustrated in figure 2. The shear rate-dependent viscosity of a strongly shear-thinning xanthan gum solution measured in a rectangular microchannel by imposing the flow rate and monitoring the wall shear stress is shown in figure 2(a) (reproduced from Pipe et al., 2008). Using high pressure syringe pumps, wall shear rates up to $\dot{\gamma} = 30000\,\mathrm{s}^{-1}$ were obtained. Good agreement is found with measurements from conventional rotational rheometers and we note that the microfluidic device is able to probe shear rates at least an order of magnitude greater than is achievable in the macroscale geometries, which are typically constrained by the onset of inertial instabilities. MicroPIV measurements of the velocity profile in microchannel flows of a shear-banding wormlike micellar solution are presented in figure 2(b) (reproduced from Masselon et al., 2008). The progressive deviation in the velocity profile from the parabolic profile expected for a constant viscosity Newtonian fluid is evident as the driving pressure is increased. These local velocity measurements can be used to determine the flow curve shown in figure 2(c) and the results are found to agree well with macro-scale cone and plate measurements for shear rates $\dot{\gamma} < 10\,\mathrm{s}^{-1}$ before the onset of the shear stress plateau.

2.2 Range of operation

Any of the techniques outlined in 2.1 can be used for measuring the viscosity of constant viscosity aqueous solutions. Certain methods are also capable of measuring the viscosity of non-Newtonian liquids where η may vary as a function of the imposed shear rate (Srivastava and Burns, 2006; Kang et al., 2005; Degré et al., 2006; Guillot et al., 2006; Masselon et al., 2008; Pipe et al.,

Preprint

2008). Some designs impose restrictions on the types of fluids which can be measured, and may require liquids with a sufficiently large surface tension (Srivastava et al., 2005), ionic liquids (Lin et al., 2007) or two immiscible liquids (Guillot et al., 2006); devices constructed using PDMS are limited to liquids which do not react with or swell the PDMS elastomer (Han et al., 2007).

The viscosity - shear rate parameter space which can be explored depends on the device geometry, how the flow is driven and the measuring technique. When the flow is pressure driven and the flow rate is measured the chief limitations on the shear rate range are the dynamic range of the image capturing system, the driving pressure and the mechanical strength of the device; fluids with shear viscosities $0.001 - 10\,\mathrm{Pa\,s}$ have been measured over a range of shear rates $10^{-1} - 10^{3}\,\mathrm{s}^{-1}$ (Srivastava and Burns, 2006; Degré et al., 2006; Guillot et al., 2006; Masselon et al., 2008). For systems in which the flow rate is imposed and the pressure drop is measured, the channel geometry combined with the accuracy and full scale of the pressure sensors are the determining factors in the range of shear rates which can be explored for a given sample viscosity (Pipe et al., 2008). Shear rates up to $\dot{\gamma} = 10^{6}\,\mathrm{s}^{-1}$ were explored by Kang et al. (2005) for a dilute polymer solution and at such large deformation rates the onset of polymer degradation was observed.

The effects of viscous heating are characterized by the Nahme number $\mathrm{Na} = \eta\beta\dot{\gamma}^2 d^2/(kT)$, where k is the thermal conductivity, T is the temperature and $\beta = \partial(\log\eta)/\partial(\log T)$ is the logarithmic derivative of viscosity with temperature or 'thermal sensitivity', and can be considered negligible when $\mathrm{Na} \ll 1$. Thus, since $\mathrm{Na} \sim d^2$, microfluidic devices offer a significant advantage over conventional macroscopic rheometers when measuring material properties at large deformation rates (Pipe et al., 2008).

Preprint

Besides fluid degradation and viscous heating, the upper limit on the shear rate that can be imposed is governed by the loss of viscometric flow beyond a critical Reynolds number $\mathrm{Re_c}$ and the transition from laminar to turbulent flow. As discussed in the review by Obot (2002), the experimental evidence so far suggests that the transition to turbulence in smooth walled microchannels occurs at $\mathrm{Re_c} \sim 2000$, comparable to the usual value for macroscale flows. Turbulent fluctuations can also contribute substantially to polymer degradation in the device (Vanapalli et al., 2006).

2.3 Further considerations

Certain fluids can show significant changes in viscosity for small changes in temperature. Thus the ability to impose a well defined temperature on the device is an important consideration when trying to accurately determine fluid viscosity and silicon-based devices are preferable here to poor thermal conductors such as PDMS elastomers. Indeed, a well controlled thermal environment may be critical for biological fluids where the biological integrity of the fluid is dependent on being kept at physiological temperature (Srivastava et al., 2005; Han et al., 2007). A further issue of particular importance when using biological fluids is that of sample contamination and, to avoid time consuming cleaning between tests, disposable devices may be desirable. Thus in this case the cost of microfluidic viscometry systems can be a key factor (Srivastava et al., 2005; Han et al., 2007).

The microfluidic systems presented by Srivastava et al. (2005), Lin et al. (2007) and Han et al. (2007) are able to function using sample volumes on the order of nanolitres, offering a $\sim 10^6$ reduction in the required sample volume

Preprint

compared to conventional viscometric techniques. This is particularly advantageous when dealing with biological samples where large volumes may not be available. Conversely, microfluidic devices involving syringe pumps and connecting tubing typically require larger volumes in the range $100\,\mu$l$-10\,$ml in order to fill the system and establish steady flow conditions (Pipe et al., 2008).

Finally we note that the presence of apparent wall slip in capillary flow may be assessed either directly or indirectly depending on the system. μPIV measurements (Degré et al., 2006; Guillot et al., 2006; Masselon et al., 2008) allow the velocity profile in the near-wall region to be observed and the effects of wall slip may be evaluated independently of the viscosity (Degré et al., 2006). If the local velocity profile is not known, apparent wall slip can be deduced indirectly using microchannels with different channel dimensions (Kang et al., 2005; Pipe et al., 2008) or by comparison with measurements from other experimental techniques (Guillot et al., 2006).

3 Microfluidic stagnation point flows

The vorticity-free state of the flow near a stagnation point can result in large extensional deformation and orientation of the microstructural components of complex fluids (Frank et al., 1971; Fuller and Leal, 1980; Fuller et al., 1987; Schoonen et al., 1998). This non-equilibrium microstructural configuration results in an increase in the *extensional viscosity* η_{e} of the fluid beyond the Trouton limit $\eta_{\mathrm{e}} = 3\eta$ or $\eta_{\mathrm{e}} = 4\eta$ expected in homogeneous uniaxial or planar extensional flows, respectively (Bird et al., 1987). With the notable exception of the Rheometrics RFX opposed nozzles rheometer (Fuller et al., 1987), information on the extensional properties is usually extracted by monitoring the

Preprint

flow birefringence in the region of the stagnation point (Fuller, 1990). Due to the high spatial resolution that is achievable, microfluidic geometries combined with modern microscopic imaging platforms are, in principle, well suited to exploring the optical properties of flows in the region of stagnation points and extracting rheological information.

A generic sketch of a microfluidic stagnation point flow is shown in figure 1(b). Currently two fundamental configurations for exploring these flows have been proposed: microfluidic implementations of the four roll mill (Hudson et al., 2004; Lee et al., 2007) and the 'cross slot' flow geometry (Pathak and Hudson, 2006; Arratia et al., 2006, 2008). Microfluidic analogues of four roll mill devices allow rotational as well as irrotational flows to be established with varying degrees of vorticity (Hudson et al., 2004; Lee et al., 2007) and the behaviour of macromolecules in flows with mixed shear and elongational characteristics can potentially be investigated. However, while flow fields have been validated experimentally and numerically for Newtonian liquids in these devices, so far no measurements of the bulk extensional properties of complex liquids have been reported in these geometrues due to the difficulty in measuring the global pressure drop or stress field in such devices.

The microfluidic cross-slot device developed by Pathak and Hudson (2006) was used to study the extensional rheology of semi-dilute surfactant solutions. The very high stress-optical coefficient of wormlike micellar systems enables spatially-resolved birefringence measurements near the stagnation point (figure 3(a)) and the elongational flow leads to the formation of a 'birefringent strand' of highly-aligned material along the centerline of the outflow region of the device (Harlen et al., 1992).

Preprint

Strong deformation of the microstructure in such flows generate large tensile stresses in a viscoelastic fluid that can ultimately lead to a steady symmetry-breaking instability followed at higher De by the onset of time-dependent flow (Arratia et al., 2006). This symmetry-breaking bifurcation has also recently been simulated by (Poole et al., 2007); as shown in figure 3(b) the symmetric Newtonian viscous flow observed at low flow rates (upper left image) undergoes a transition at Deborah numbers De ~ 1 to an increasingly asymmetric flow, with highly localized viscoelastic stresses along the outflow centerline.

The 'flow focusing' characteristics of the planar extensional flow generated in microfluidic cross-slot geometries has also recently been used to investigate the necking and pinch-off of immiscible Newtonian and polymeric fluid filaments (Steinhaus et al., 2007; Arratia et al., 2008). In this geometry (see figure 3(c)) three of the flow channels supply the two immiscible fluids (here the viscoelastic core fluid is supplied from the lefthand input and a mineral oil is supplied from the upper and lower arms), and there is only one outflow. The outer (lower viscosity) fluid relieves the shear induced at the microchannel walls by the usual no-slip boundary condition. Experiments with immiscible Newtonian fluids show breakup into a series of monodisperse drops with dimensions controlled by the geometry, flow rate and viscosity ratio (Link et al., 2004). However, when the inner fluid is viscoelastic the filament length and time to pinch-off is controlled by the molecular weight of the polymeric chains and the elastocapillary number of the solution (Steinhaus et al., 2007). By monitoring the filament diameter $h(t)$ and constructing a force balance based on the viscous, elastic and capillary driving forces the steady extensional viscosity η_{e} of the polymer solution can be estimated as a function of the extensional rate $\dot{\epsilon} = (-2/h)(\mathrm{d}h/\mathrm{d}t)$ in the filament. For flow of a Newtonian outer fluid with

shear viscosity η_A at a flow rate Q_A, the extensional viscosity of the inner polymeric fluid is given by $\eta_e = 3\eta_A Q_A/(\dot{\epsilon} w^2 d)$ (Arratia et al., 2008).

4 Microfluidic contraction flows

Contraction flows have been used for many years to investigate the extensional properties of complex liquids in macroscale flow geometries (Cogswell, 1972; Williams and Williams, 1985; Binding, 1988; James et al., 1990) by relating the measured pressure drop across a contraction to the imposed flow rate. Two main approaches can be identified: experiments using abrupt contractions which are easier to design and build and those using hyperbolic contractions which provide a better approximation to a uniform extension rate (Everage and Ballman, 1978). Macroscopic studies are typically restricted to viscous liquids $\eta \gtrsim 1\,\mathrm{Pa\,s}$ because the extension rates $O(1000\,\mathrm{s}^{-1})$ needed to probe the elongational behaviour of low viscosity solutions $\eta \sim 0.001\,\mathrm{Pa\,s}$ often result in large inertial stresses which dominate the viscous contribution to the total pressure drop across the contraction plane. Thus microfluidic devices - which are capable of imposing large deformation rates while remaining in low inertia flow regimes - offer the potential to apply these techniques to low viscosity polymer solutions. Excepting early work by James and Saringer (1980) who used precision-machined hyperbolic axisymmetric contraction geometries with dimensions of $O(100\,\mu\mathrm{m})$, it should be noted that in contrast to macroscopic experiments, microfluidic studies of contraction flows have to date been principally limited to planar geometries.

It must be noted that contraction flows are of mixed kinematic type and typically contain both strong shear and elongational components. This is

Preprint

important as coupling between the extensional ('irrotational') and shearing ('rotational') deformations may lead to a significantly different microstructural response compared to a pure irrotational extensional deformation. Thus we emphasize that estimates of extensional material properties derived from contraction flows are only *apparent* measures (Petrie, 2006). This limitation notwithstanding, such flows can provide important insight into how complex fluids behave in mixed flows with strong elongational components, which are highly relevant to industrial applications such as inkjetting and of academic interest in their own right.

Experiments with dilute and semi-dilute polymer solutions have shown that measurements of the pressure drop across planar contraction geometries (see figure 1(c)) increase linearly at low flow rates corresponding to $\mathrm{De} < 0.5$ but that as the flow flow rates increase beyond $\mathrm{De} > 0.5$ viscoelastic effects lead to an enhanced pressure drop (Groisman et al., 2003; Rodd et al., 2005; Kang et al., 2006; Pipe and McKinley, In preparation). From an appropriate global force balance across the contraction (Cogswell, 1972; Binding, 1988) it is possible to evaluate an apparent elongational viscosity which can be referenced against the independently measured steady-shear viscosity to evaluate the Trouton ratio of a complex fluid. The apparent extensional viscosity is found by separating the pressure drop due to shear stresses from that due to extensional stresses. Relating the pressure drop across the contraction (due to the presence of the polymer chains undergoing extension) to the first normal stress difference N_1, combined with a suitable estimate of the extension rate $\dot{\epsilon}$, gives the apparent extensional viscosity $\eta_e = N_1/\dot{\epsilon}$ and hence the Trouton ratio. For viscoelastic liquids, care must be taken to ensure that the desired kinematics in the device are also achieved, because the coupling between the

enhanced stress field arising from strain-hardening and the local kinematics can also lead to rearrangement of the converging streamlines upstream of the contraction for De ~ 1. Representative measurements for solutions of flexible polyethylene oxide (PEO) polymer chains and for a semi-rigid hydroxyethylcellulose (HEC) solution are shown in Figure 4(a)[reproduced from (Kang et al., 2006)]. Independent measurements of the apparent extensional viscosity in a spinline rheometer show that as the total Hencky strain imposed on the sample is increased, the Trouton ratios diverge from the expected (constant) Newtonian value, with the flexible chain system showing strain-hardening due to molecular elongation; by contrast the semi-rigid molecules shows a progressive strain-softening as a result of increasing molecular flow alignment. These deviations lead to substantial differences in the flow characteristics through a microfabricated contraction geometry (with 36° convergence angle) and local strain-hardening eventually leads to the generation of vortices as shown in the lower portion of Figure 4(a). Similar observations have now been made with a range of different fluids in a number of different converging channel designs (Groisman et al., 2003; Rodd et al., 2005; Kang et al., 2006; Rodd et al., 2007; Pipe and McKinley, In preparation).

The mean extensional Hencky strain imposed on a fluid element flowing along the centerline of the contraction is $\epsilon = \ln(w_1/w_2)$, where w_1 is the upstream width and w_2 the width at the throat (see figure 1(c)), and can be calculated independently of the form of the contraction. The applied rate of extension $\dot{\epsilon}$, however, is governed by the flow rate and the shape of the converging section and can be written in the form $\dot{\epsilon} \sim Q\,(w_1 - w_2)/(w_1 w_2\, L\, d)$, where for hyperbolic contractions L is the length of the contraction and for aprupt contractions L is selected by the flow. Different shapes of contraction have been investi-

gated including abrupt (Rodd et al., 2005, 2007), angled (Kang et al., 2006) and hyperbolic geometries (Pipe and McKinley, In preparation). Numerical calculations and experimental measurements of the local velocity fields in hyperbolic contractions can be used in combination to investigate how well flows with constant extension rate along the centre line can be realized in such devices. In Figure 4(b) we show a detailed comparison for steady flow of water through hyperbolic contractions with Hencky strain $\epsilon = 1$ and $\epsilon = 2$ (Oliveira et al., 2007). The colors indicate contours of constant axial velocity through the contraction and spatial derivatives of this velocity field with respect to axial and lateral positions give the local extensional and shearing contributions to the rate of material deformation. The effects of shear induced by the no slip boundary condition are localized to the hyperbolic channel walls. With care, very good quantitative agreement between numerical computation and experimental measurement can be achieved and this enables computational design explorations to be performed in advance for optimizing the performance of microfluidic rheometers for measuring elongational properties of liquids in well defined extensional kinematic fields.

Measurements of the pressure drop across a symmetric contraction - expansion geometry using a series of low viscosity polymer solutions (Pipe and McKinley, In preparation) as a function of flow rate are shown in figure 4(c). For the viscous Newtonian solvent (a glycerin/water mixture) the pressure drop increases linearly with flow rate and the extensional viscosity (or Trouton ratio) remains constant. However, as the concentration of polymer is increased, the characteristic relaxation time λ of the solution increases and the enhanced extra pressure drop across the contraction leads to substantial increases in the apparent planar extensional viscosity η_{e} as a function of the extensional

Preprint

rate through the device. At low flow rates the sensitivity of the extensional rheometer is limited by the background noise fluctuations in the pressure sensors and precision in control of the imposed flow rate; because the extensional viscosity involves a ratio of the measured pressure drop and the flow rate this leads to rapid increase in the magnitude of the error bars at low flow rates.

At moderate Reynolds numbers there is an additional enhancement to the total pressure drop across the contraction - expansion even for Newtonian fluids due to the presence of inertia Re > 10 (Rodd et al., 2005; Oliveira et al., 2007). Experiments and finite element calculations have shown that this is accompanied by the formation of steady and three-dimensional vortex structures downstream of the contraction (Rodd et al., 2005; Tsai et al., 2007; Oliveira et al., 2007, 2008). It is thus essential to ensure that inertial corrections are accounted for and that the elasticity number El = De/Re of proposed microfluidic rheometric devices remains suitably large to ensure that the elastic effects one seeks to measure dominate over inertial non-idealities.

5 Perspectives

The arrival of microfluidic technology has not only increased the need for rheological information about the flow of non-Newtonian liquids in microscale geometries and at high deformation rates, but has also provided a new platform for the design and testing of new rheometric devices to explore fluid rheology. While recognizing the restrictions that current (planar) microfluidic manufacturing techniques impose on the types of flow configurations that can be realized, we have shown that microfluidic systems also present a number of new opportunities for the rheologist interested in measuring material prop-

Preprint

erties in shear, shear-free and mixed kinematics.

A wide range of novel methods for measuring the steady shear viscosity of complex fluids using microfluidic capillary channels have been surveyed as well as microfluidic stagnation and contraction flows for investigating the extensional properties of complex liquids. These devices offer viable alternatives to conventional rheological characterization techniques; allowing smaller sample volumes to be used, higher deformation rates to be attained and disposable devices to be made cheaply. These rheometric subystems can also (potentially) be integrated into lab-on-a-chip systems, and - in combination with microscopy or other optical techniques - they can probe the coupling between the macroscopic stress and the microstructural deformation of complex liquids. In particular, microfluidic devices show great potential to offer insights into two long-standing problems in rheology: the high shear rate response of complex liquids and the extensional behaviour of low viscosity viscoelastic liquids. A number of important technological challenges remain outstanding, including the challenge of fabricating reproducible and reliable microdevices in moderate volumes and with high yields. If the devices are flow-rate controlled (e.g. by an external syringe pump) then the principal challenge is constructing and calibrating on-chip pressure sensors with good linearity and wide dynamic range. If the system is pressure controlled then the limited dynamic range of many optical-based techniques for measuring local fluid velocity constrains the capabilities of the microfludic rheometer. The overall compliance of the device, total volume of liquid required and the nucleation/growth of microscopic air bubbles must also be considered.

For all of these reasons, calibration of the final system with a simple Newtonian fluid (with constant viscosity) which has been independently tested in

Preprint

macroscale experiments is highly recommended. The 'open' nature of the flow geometry (i.e. the presence of inflow and outflow boundaries) is fundamentally different from many conventional torsional rheometers. Computational analysis of the steady three-dimensional flow fields that are typically present in microfluidic devices is also desirable. To date almost all such numerical studies have been performed with Newtonian constitutive models only, and similar analyses for more complex rheological equations of state (incorporating for example shear-thinning in the viscosity, fluid viscoelasticity and/or the presence of a yield stress) presents a golden opportunity for computational rheologists. Many of the complex fluids studied experimentally have exhibited the onset of either steady flow transitions or three-dimensional time-dependent instabilities; and the ability to rationally design modifications to devices (such as optimizing aspect ratios, minimizing flow inhomogeneities and reducing stress concentrations near sharp corners) would prove invaluable. On the macroscale, the combination of bulk rheometry with local rheo-optical probes (e.g. birefringence, dichroism and scattering techniques over a wide range of wavelengths) in the 1980s and beyond greatly expanded the impact and microstructural insight that could be attained from rheometry. Microfluidic rheometry is naturally predisposed to similar evolutionary developments because of the ready availability of high resolution imaging platforms with many different modes of optical illumination. It is to be anticipated that integrated microfluidic devices combining full-field diagnostic techniques such as micro particle image velocimetry and flow-induced birefringence with mechanical measurement of stresses or pressures will be developed in the coming years.

Preprint

Acknowledgements

CJP was supported by a Chinese Academy of Sciences Research Fellowship for International Young Researchers and would like to graciously thank Prof. Z. Li and her group for their help and warm welcome.

References

Anna, S. L., Bontoux, N., Stone, H. A., 2003. Formation of dispersions using "flow focusing" in microchannels. Appl. Phys. Lett. 82 (3), 364–366.

Arratia, P. E., Gollub, J. P., Durian, D. J., 2008. Polymeric filament thinning and breakup in microchannels. Phys. Rev. E 77, 036309.

Arratia, P. E., Thomas, C. C., Diorio, J., Gollub, J. P., 2006. Elastic instabilities of polymer solutions in cross-channel flow. Phys. Rev. Lett. 96, 144502.

Barnes, H. A., 1995. A review of the slip (wall depletion) of polymer solutions, emulsions and particle suspensions in viscometers: its cause, character, and cure. J. Non-Newtonian Fluid Mech. 56 (3), 221–251.

Batchelor, G. K., 1967. An Introduction to Fluid Mechanics. Cambridge University Press.

Bausch, A. R., Ziemann, F., Boulbitch, A. A., Jacobson, K., Sackmann, E., 1998. Local measurements of viscoelastic parameters of adherent cell surfaces by magnetic bead microrheometry. Biophys. J. 75, 2038–2049.

Binding, D. M., 1988. An approximate analysis for contraction and converging flows. Journal of Non-Newtonian Fluid Mechanics 27 (2), 173–189.

Bird, R. B., Armstrong, R. C., Hassager, O., 1987. Dynamics of Polymeric Liquids, Vol. 1, 2nd Edition. John Wiley and Sons.

Brau, R. R., Ferrer, J. M., Lee, H., Castro, C. E., Tam, B. K., Tarsa, P. B.,

Preprint

Matsudaira, P., Boyce, M. C., Kamm, R. D., Lang, M. J., 2007. Passive and active microrheology with optical tweezers. Journal of Optics A: Pure and Applied Optics 9 (8), S103–S112.

Chen, Y., Graham, M., de Pablo, J., Randall, G., Gupta, M., Doyle, P., 2004. onformation and dynamics of single DNA molecules in parallel-plate slit microchannels. Phys. Rev. E 90 (6), 060901.

Choi, M. C., Pfohl, T., Wen, Z., Li, Y., Kim, M. W., Israelachvili, J. N., Safinya, C. R., 2004. Ordered patterns of liquid crystal toroidal defects by microchannel confinement. PNAS 101 (50), 17340–17344.

Clasen, C., McKinley, G. H., 2004. Gap-depedent microrheometry of complex liquids. J. Non-Newtonian Fluid Mech. 124, 1–10.

Cogswell, F. N., 1972. Converging flow of polymer melts in extrusion dies. Polym. Eng. Sci. 12 (1), 64–73.

Colin, S., 2005. Rarefaction and compressibility effects on steady and transient gas flows in microchannels. Microfluid Nanofluid 1, 268–279.

Connelly, R. W., Greener, J., 1985. High-shear viscometry with a rotational parallel-disk device. Journal of Rheology 29 (2), 209–226.

Degré, G., Joseph, P., Tabeling, P., 2006. Rheology of complex fluids by particle image velocimetry in microchannels. Appl. Phys. Lett. 89 (024104), 1–3.

Dhinojwala, A., Granick, S., 1997. Micron-gap rheo-optics with parallel plates. J. Chem. Phys. 107 (20), 8664–8667.

Duda, J. L., Klaus, E. E., Lin, S.-C., 1988. Capillary viscometry study of non-Newtonian fluids: Influence of viscous heating. Ind. Eng. Chem. Res. 27, 352–361.

Everage, A., Ballman, R., 1978. The extensional flow capillary as a new method for extensional viscosity measurement. Nature 273, 213–215.

Preprint

Frank, F. C., Keller, A., Mackley, M. R., 1971. Polymer chain extension produced by impinging jets and its effect on polyethylene solution. Polymer 12, 467–473.

Fuller, G. G., 1990. Optical rheometry. Annu. Rev. Fluid Mech. 22, 387–417.

Fuller, G. G., Cathey, C. A., Hubbard, B., Zebrowski, B. E., 1987. Extensional viscosity measurements for low-viscosity fluids. J. Rheol. 31 (3), 235–249.

Fuller, G. G., Leal, L. G., 1980. Flow birefringence of dilute polymer solutions in two-dimensional flows. Rheol. Acta 19, 580–600.

Granick, S., Zhu, Y., Lee, H., 2003. Slippery questions about complex fluids flowing past solids. Nature Materials 2, 221–227.

Groisman, A., Enzelberger, M., Quake, S. R., 2003. Microfluidic memory and control devices. Science 300, 955–958.

Guillot, P., Panizza, P., Joanicot, J.-B. S. M., Colin, A., 2006. Viscosimeter on a microfluidic chip. Langmuir 22, 6438–6445.

Han, Z., Tang, X., Zheng, B., 2007. A pdms viscometer for microliter newtonian fluid. J. Micromech. Microeng. 17, 1828–1834.

Hansen, C., Quake, S. R., 2003. Microfluidics in structural biology: smaller, faster... better. Curr. Opin. Struct. Biol. 13, 538–544.

Harlen, O., Hinch, E., Rallison, J., 1992. Birefringent pipes: The steady flow of a dilute polymer solution near a stagnation point. J. Non-Newtonian Fluid Mech. 44, 229–265.

Higashitani, K., Pritchard, W., 1972. Kinematic calculation of intrinsic errors in pressure measurements made with holes. Trans. Soc. Rheol. 16 (4), 687–696.

Hudson, S. D., Phelan, F. R., Handler, M. D., Cabral, J. T., Migler, K. B., Amis, E. J., 2004. Microfluidic analog of the four-roll mill. Appl. Phys. Lett. 85 (2), 335–337.

Preprint

Hur, J. S., Shaqfeh, E. S. G., Babcock, H. P., Smith, D. E., 2001. Dynamics of dilute and semidilute dna solutions in the start-up of shear flow. J. Rheol. 45 (2), 421–450.

James, D. F., Chandler, G. M., Armour, S. J., 1990. A converging channel rheometer for the measurement of extensional viscosity. Journal of Non-Newtonian Fluid Mechanics 35 (2-3), 421–443.

James, D. F., Saringer, J. H., 1980. Extensional flow of dilute polymer solutions. J. Fluid Mech. 97 (4), 655–671.

Kang, K., Koelling, K. W., Lee, L. J., 2006. Microdevice end pressure evaluations with bagley correction. Microfluid Nanofluid 2, 223–235.

Kang, K., Lee, L. J., Koelling, K. W., 2005. High shear microfluidics and its application in rheological measurement. Exp. Fluids 38, 222–232.

Larson, R. G., 1999. The structure and rheology of complex fluids. Oxford University Press.

Larson, R. G., 2007. Going with the flow. Science 318, 57–58.

Lauga, E., Brenner, M. P., Stone, H. A., 2007. Microfluidics: the no-slip boundary condition. In: Tropea, C., Yarin, A. L., Foss, J. F. (Eds.), Handbook of Experimental Fluid Dynamics. Springer.

Lee, J., Tripathi, A., 2005. Intrinsic viscosity of polymers and biopolymer measured by microchip. Anal. Chem. 77 (22), 7137–7147.

Lee, J. S., Dylla-Spears, R., Teclemariam, N. P., Muller, S. J., 2007. Microfluidic four-roll mill for all flow types. Appl. Phys. Lett. 90, 074103.

Lin, Y.-Y., Lin, C.-W., Yang, L.-J., Wang, A.-B., 2007. Micro-viscometer based on electrowetting on dielectric. Electrochimica Acta 52, 2876–2883.

Link, D. R., Anna, S. L., Weitz, D. A., Stone, H. A., 2004. Geometrically mediated breakup of drops in microfluidic devices. Phys. Rev. Lett. 92 (5), 054503.

Preprint

MacKintosh, F. C., Schmidt, C. F., 1999. Microrheology. Curr. Opin. Colloid Interface Sci. 4, 300–307.

Macosko, C. W., 1994. Rheology: Principles, Measurements and Applications. Wiley-VCH.

Marrian, C. R. K., Tennant, D. M., 2003. Nanofabrication. J. Vac. Sci. Technol. A 21 (5), 207–215.

Masselon, C., Salmon, J.-B., Colin, A., 2008. Nonlocal effects in flows of worm-like micellar solutions. Phys. Rev. Lett. 100, 038301.

McKenna, G. B., 2006. Commentary on rheology of polymers in narrow gaps. Eur. Phys. J. E 19 (1), 101–108.

Meiners, J.-C., Quake, S. R., 2000. Femtonewton force spectroscopy of single extended dna molecules. Phys. Rev. Lett. 84 (21), 5014–5017.

Meyer, E., Overney, R., Dransfeld, K., Gyalog, T., 1998. Nanoscience: Friction and Rheology on the Nanometer Scale, Vol. 1. Vol. 1. World Scientific, Singapore.

Mukhopadhyay, A., Granick, S., 2001. Micro- and nanorheology. Curr. Opin. Colloid Interface Sci. 6, 423–429.

Ng, J. M. K., Gitlin, I., Stroock, A. D., Whitesides, G. M., 2002. Components for integrated poly(dimethylsiloxane) microfluidic systems. Electrophoresis 23, 3461–3473.

Obot, N. T., 2002. Toward a better understanding of friction and heat/mass transfer in microchannels– a literature review. Microscale Thermophys. Eng. 6 (3), 155–173.

Oliveira, M. S. N., Alves, M. A., Pinho, F. T., McKinley, G. H., 2007. Viscous flow through microfabricated hyperbolic contractions. Experiments in Fluids 43 (2), 437–451.

Oliveira, M. S. N., Rodd, L. E., McKinley, G. H., Alves, M. A., 2008. Simula-

Preprint

tions of extensional flow in microrheometric devices. Microfluid Nanofluid In press.

Pathak, J. A., Hudson, S. D., 2006. Rheo-optics of equilibrium polymer:solutions: wormlike micelles in elongational flow in a microfluidic cross-slot. Macromolecules 39, 8782–8792.

Perkins, T. T., Smith, D. E., Chu, S., 1997. Single polymer dynamics in an elongational flow. Science 276, 2016–2021.

Petrie, C. J. S., 2006. Extensional viscosity: A critical discussion. J. Non-Newtonian Fluid Mech. 137, 15–23.

Pipe, C. J., Majmudar, T. S., McKinley, G. H., 2008. High shear rate viscometry. Rheol. Acta.

Pipe, C. J., McKinley, G. H., In preparation. A microfluidic extensional viscosity indexer. Microfluid Nanofluid.

Poole, R. J., Alves, M. A., Oliveira, P. J., 2007. Purely elastic flow asymmetries. Phys. Rev. Lett. 99, 164503.

Quake, S. R., Scherer, A., 2000. From micro- to nanofabrication with soft materials. Science 290, 1536–1540.

Rodd, L. E., Cooper-White, J. J., Boger, D. V., McKinley, G. H., 2007. Role of the elasticity number in the entry flow of dilute polymer solutions in microfabricated contraction geometries. J. Non-Newtonian Fluid Mech. 143, 170–191.

Rodd, L. E., Scott, T. P., Boger, D. V., Cooper-White, J. J., McKinley, G. H., 2005. The inertio-elastic planar entry flow low-viscosity elastic fluids in microfabricated geometries. J. Non-Newtonian Fluid Mech. 129, 1–22.

Schoonen, J. F. M., Swartjes, F. H. M., Peters, G. W. M., Baaijens, F. P. T., Meijer, H. E. H., 1998. A 3d numerical/experimental study on a stagnation flow of a polyisobutylene solution. J. Non-Newtonian Fluid Mech. 79, 529–

Preprint

561.

Shaqfeh, E. S. G., 2005. The dynamics of single-molecule dna in flow. J. Non-Newtonian Fluid Mech. 130 (1), 1–28.

Shojaei-Zadeh, S., Anna, S. L., 2006. Role of surface anchoring and geometric confinement on focal conic textures in smectic-a liquid crystals. Langmuir 22, 9986–9993.

Smith, D. E., Babcock, H. P., Chu, S., 1999. Single polymer dynamics in steady shear flow. Science 283, 1724–1727.

Squires, T. M., Quake, S. R., 2005. Microfluidics: Fluid physics at the nanoliter scale. Rev. Mod. Phys. 77, 977–1026.

Srivastava, N., Burns, M. A., 2006. Analysis of non-newtonian liquids using a microfluidic capillary viscometer. Anal. Chem. 78, 1690–1696.

Srivastava, N., Davenport, R. D., Burns, M. A., 2005. Nanoliter viscometer for analyzing blood plasma and other liquid samples. Anal. Chem. 77, 383–392.

Starrs, L., Bartlett, P., 2003. One- and two-point micro-rheology of viscoelastic media. J. Phys.: Condens. Matter 15 (251-256).

Stein, D., van der Heyden, F. H. J., Koopmans, W. J. A., Dekker, C., 2006. Pressure-driven transport of confined DNA polymers in fluidic channels. PNAS 103 (43), 15853–15858.

Steinhaus, B., Shen, A., Sureshkumar, R., 2007. Dynamics of viscoelastic fluid filaments in microfluidic devices. Phys. Fluids 19 (7), 073103.

Stone, H. A., Stroock, A. D., Ajdari, A., 2004. Engineering flows in small devices: microfluidics toward lab-on-a-chip. Annu. Rev. Fluid Mech. 36, 381–411.

Stroock, A. D., Dertinger, S. K. W., Ajdari, A., Mezic, I., Stone, H. A., Whitesides, G. M., 2002. Chaotic mixer for microchannels. Science 295 (647-651).

Thorsen, T., Roberts, R. W., Arnold, F. H., Quake, S. R., 2001. Dynamic

Preprint

pattern formation in a vesicle-generating microfluidic device. Phys. Rev. Lett. 86 (18), 4163–4166.

Tsai, C.-H., Chen, H.-T., Wang, Y.-N., Lin, C.-H., Fu, L.-M., 2007. Capabilities and limitations of 2-dimensional and 3-dimensional numerical methods in modeling the fluid flow in sudden expansion microchannels. Microfluid Nanofluid 3 (1), 13–18.

Vanapalli, S. A., Ceccio, S. L., Solomon, M. J., 2006. Universal scaling for polymer chain scission in turbulence. Proc. Nat. Acad. Sci. 103 (45), 16660–16665.

Voronov, R. S., Papavassiliou, D. V., Lee, L. L., 2008. Review of fluid slip over superhydrophobic surfaces and its dependence on the contact angle. Ind. Eng. Chem. Res. In press.

Waigh, T. A., 2005. Microrheology of complex fluids. Rep. Prog. Phys. 68, 685–742.

Weitz, D. A., Pine, D. J., 1992. Diffusing wave spectroscopy. In: Brown, W. (Ed.), Dynamic Light Scattering. Oxford University Press.

White, F. M., 1991. Viscous fluid flow, 2nd Edition. McGraw-Hill Science.

Whitesides, G. M., 2006. The origins and the future of microfluidics. Nature 442 (7101), 368–373.
URL `http://dx.doi.org/10.1038/nature05058`

Williams, P. R., Williams, R. W., 1985. On the planar extensional viscosity of mobile liquids. J. Non-Newtonian Fluid Mech. 19, 53–80.

Zimmerman, W. B., Rees, J. M., Craven, T. J., 2006. Rheometry of non-Newtonian electrokinetic flow in a microchannel T-junction. Microfluid Nanofluid 2, 481–492.

Preprint

Figure captions

Figure 1: Overview of microfluidic devices for investigating rheometry on a chip: (a) capillary slit devices for measuring shear viscosity; (b) stagnation point flows in a 'cross-slot' for measuring extensional properties; and (c) two different possible contraction flows (an abrupt contraction - expansion and a planar hyperbolic contraction) also used for investigating extensional properties. Dimensions where given are explained in the text.

Figure 2: Measurements of shear viscosity in microfluidic capillary flows: (a) Viscosity η as a function of shear rate $\dot{\gamma}$ for a strongly shear-thinning 0.3% aqueous xanthan gum solution measured using a microfluidic capillary viscometer as well as conventional cone and plate and plate-plate rotational devices (reproduced from Pipe et al., 2008). (b) Velocity profiles for flow of a cetylpyridinium chloride/sodium salicylate wormlike micellar solution through a rectilinear microfluidic channel at driving pressures $\bigcirc$ 200, $\triangleright$ 300, $\square$ 400, $\diamond$ 500, and $\triangle$ 600 mbar; (c) flow curve of shear stress σ against shear rate $\dot{\gamma}$ calculated from the velocity profiles (hollow symbols) and shown with cone and plate geometry measurements ($\times$) (reproduced from Masselon et al., 2008).

Figure 3: Stagnation point flows used to investigate extensional properties: (a) False color images of optical retardance $\sin\theta$ (left) and transmitted light intensity images (right) for flow of a cetylpyridinium chloride/sodium salicylate wormlike micellar solution in a cross-slot geometry at flow rates $Q = 0.1, 0.3, 0.45, 0.7$ and $0.8\,\mu$l/hour (from top to bottom). The stagnation point is indicated 'SP' and the central birefringent band signifies a high degree of microstructural alignment at large flow rates (reproduced from Pathak and

Preprint

Hudson, 2006). (b) Numerically calculated streamlines and contour plots of the normalized first normal stress difference for a Newtonian fluid and for a Maxwell fluid with $\mathrm{De} = 0.3, 0.32$ and 0.4 (a–d respectively) in a cross-slot geometry (reproduced from Poole et al., 2007). (c) Formation of a viscoelastic filament of aqueous polyacrylamide solution dispersed in mineral oil in a cross-slot geometry. The filament is shown with measurement locations (top) along with the time evolution of the local filament radius (middle) and the local extension rate in the filament (bottom) (reproduced from Arratia et al., 2008).

Figure 4: Microfluidic contraction flows: (a) The apparent Trouton ratio $\mathrm{Tr} = \eta_e/\eta_0$ for solutions of PEO and HEC measured in a spinline rheometer; the changes in the extensional rheology with increasing strain lead to transitions in the local extensional flow field in a microfluidic converging channel rheometer (reproduced from Kang et al., 2006). (b) Streamwise velocity measured experimentally (left) and calculated numerically (right) for Newtonian flow through hyperbolic contraction geometries with strains $\epsilon = 2$ (top) and $\epsilon = 1$ (bottom) (reproduced from Oliveira et al., 2007). (c) Apparent Trouton ratio $\mathrm{Tr} = \eta_{\mathrm{ext}}/\eta$ as a function of the apparent non-dimensional extension rate $\mathrm{De} = \dot{\gamma}\lambda$ for flows of dilute polyethylene oxide solutions through a symmetric hyperbolic contraction expansion (reproduced from Pipe and McKinley, In preparation).

Preprint

Figures

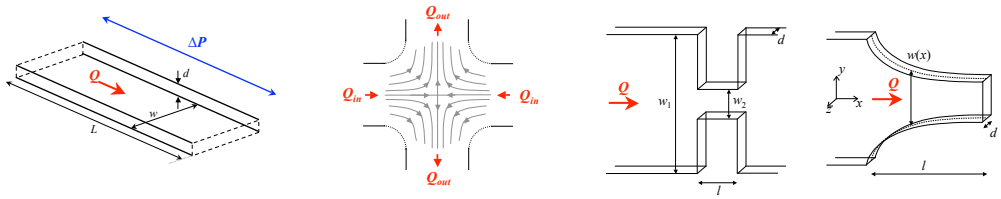

(a) Capillary

(b) Stagnation point flow

(c) Contraction geometries

Fig. 1.

Preprint

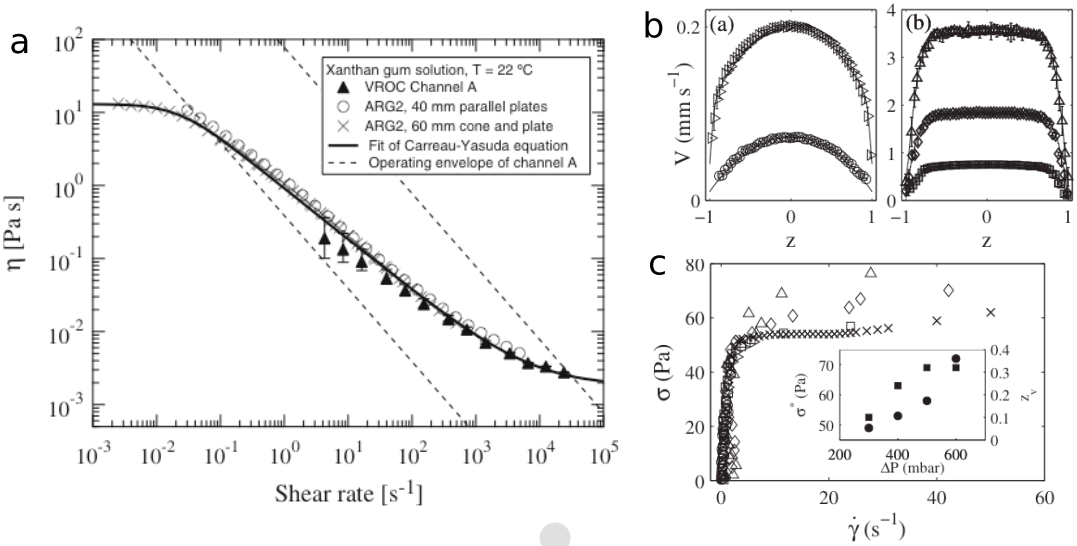

Fig. 2.

Preprint

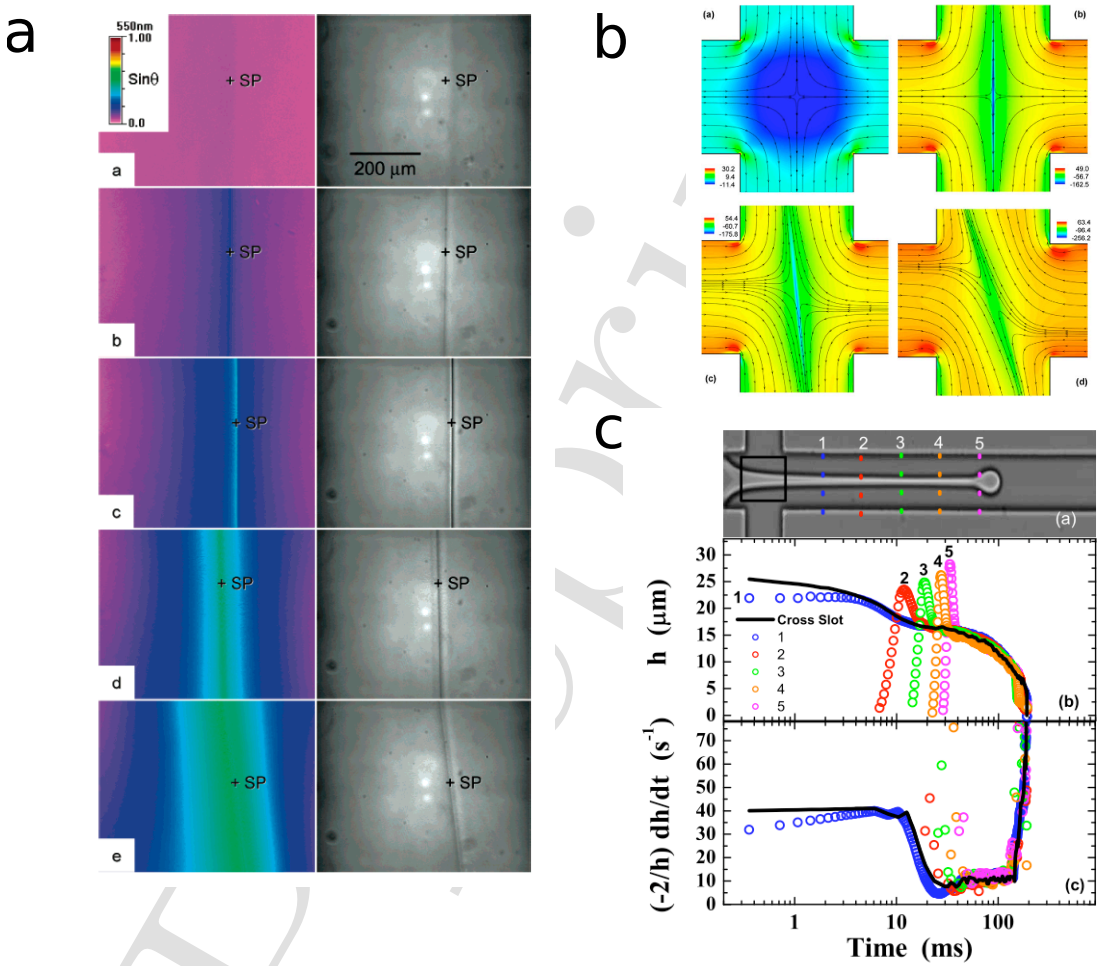
a
550nm
1.00
Sinθ
0.0
+ SP
200 µm
b
c
d
e
b
(a)
(b)
(c)
(d)
c
1
2
3
4
5
(a)
h (µm)
Cross Slot
(b)
(-2/h) dh/dt (s-1)
(c)
Time (ms)

Fig. 3.

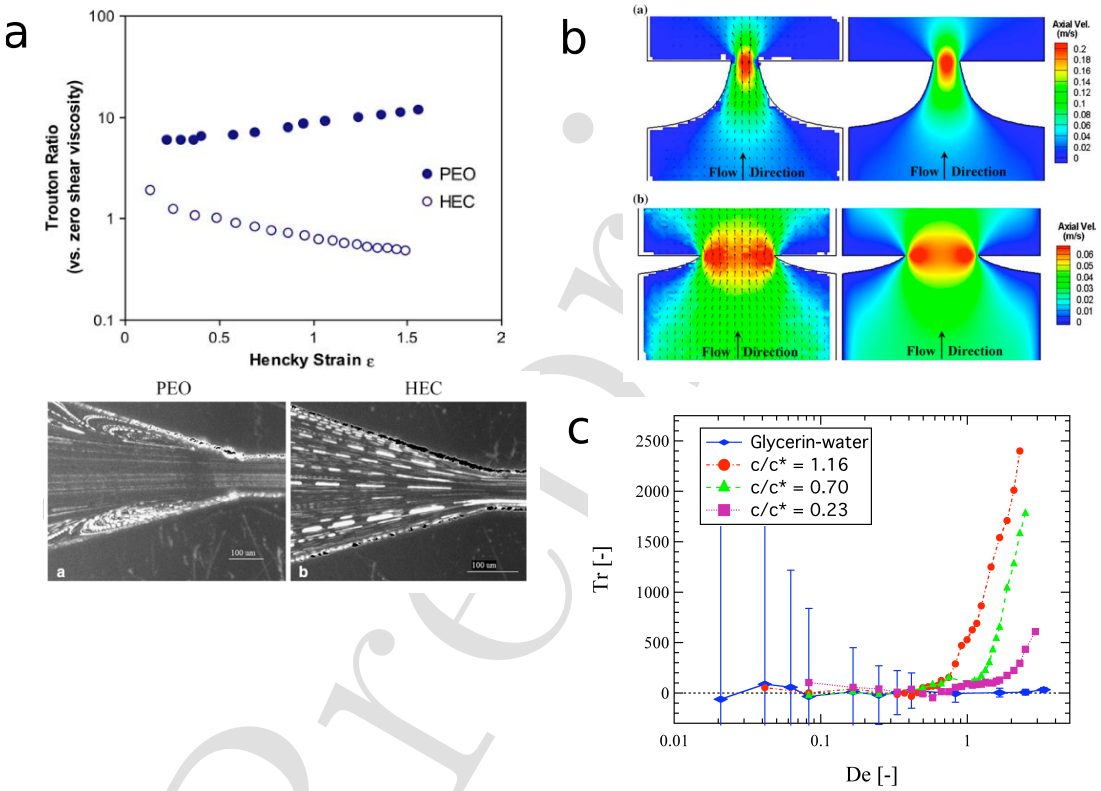
a
Trouton Ratio
(vs. zero shear viscosity)
Hencky Strain ε
PEO
HEC
PEO
HEC
b
Flow Direction
Axial Vel. (m/s)
c
Glycerin-water
c/c* = 1.16
c/c* = 0.70
c/c* = 0.23
Tr [-]
De [-]

Fig. 4.